Azimuthal di-hadron correlations in d + Au and Au + Au collisions at $\sqrt{s_{NN}} = 200$ GeV measured at the STAR detector

M. M. Aggarwal,[31] Z. Ahammed,[22] A. V. Alakhverdyants,[18] I. Alekseev,[16] J. Alford,[19] B. D. Anderson,[19] D. Arkhipkin,[3] G. S. Averichev,[18] J. Balewski,[23] L. S. Barnby,[2] S. Baumgart,[53] D. R. Beavis,[3] R. Bellwied,[51] M. J. Betancourt,[23] R. R. Betts,[8] A. Bhasin,[17] A. K. Bhati,[31] H. Bichsel,[50] J. Bielcik,[10] J. Bielcikova,[11] B. Biritz,[6] L. C. Bland,[3] B. E. Bonner,[37] J. Bouchet,[19] E. Braidot,[28] A. V. Brandin,[26] A. Bridgeman,[1] E. Bruna,[53] S. Bueltmann,[30] I. Bunzarov,[18] T. P. Burton,[3] X. Z. Cai,[41] H. Caines,[53] M. Calderón de la Barca Sánchez,[5] O. Catu,[53] D. Cebra,[5] R. Cendejas,[6] M. C. Cervantes,[43] Z. Chajecki,[29] P. Chaloupka,[11] S. Chattopadhyay,[48] H. F. Chen,[39] J. H. Chen,[41] J. Y. Chen,[52] J. Cheng,[45] M. Cherney,[9] A. Chikanian,[53] K. E. Choi,[35] W. Christie,[3] P. Chung,[11] R. F. Clarke,[43] M. J. M. Codrington,[43] R. Corliss,[23] J. G. Cramer,[50] H. J. Crawford,[4] D. Das,[5] S. Dash,[13] A. Davila Leyva,[44] L. C. De Silva,[51] R. R. Debbe,[3] T. G. Dedovich,[18] A. A. Derevschikov,[33] R. Derradi de Souza,[7] L. Didenko,[3] P. Djawotho,[43] S. M. Dogra,[17] X. Dong,[22] J. L. Drachenberg,[43] J. E. Draper,[5] J. C. Dunlop,[3] M. R. Dutta Mazumdar,[48] L. G. Efimov,[18] E. Elhalhuli,[2] M. Elnimr,[51] J. Engelage,[4] G. Eppley,[37] B. Erazmus,[42] M. Estienne,[42] L. Eun,[32] O. Evdokimov,[8] P. Fachini,[3] R. Fatemi,[20] J. Fedorisin,[18] R. G. Fersch,[20] P. Filip,[18] E. Finch,[53] V. Fine,[3] Y. Fisyak,[3] C. A. Gagliardi,[43] D. R. Gangadharan,[6] M. S. Ganti,[48] E. J. Garcia-Solis,[8] A. Geromitsos,[42] F. Geurts,[37] V. Ghazikhanian,[6] P. Ghosh,[48] Y. N. Gorbunov,[9] A. Gordon,[3] O. Grebenyuk,[22] D. Grosnick,[47] S. M. Guertin,[6] A. Gupta,[17] N. Gupta,[17] W. Guryn,[3] B. Haag,[5] A. Hamed,[43] L.-X. Han,[41] J. W. Harris,[53] J. P. Hays-Wehle,[23] M. Heinz,[53] S. Heppelmann,[32] A. Hirsch,[34] E. Hjort,[22] A. M. Hoffman,[23] G. W. Hoffmann,[44] D. J. Hofman,[8] M. J. Horner,[22] B. Huang,[39] H. Z. Huang,[6] T. J. Humanic,[29] L. Huo,[43] G. Igo,[6] P. Jacobs,[22] W. W. Jacobs,[15] C. Jena,[13] F. Jin,[41] C. L. Jones,[23] P. G. Jones,[2] J. Joseph,[19] E. G. Judd,[4] S. Kabana,[42] K. Kajimoto,[44] K. Kang,[45] J. Kapitan,[11] K. Kauder,[8] D. Keane,[19] A. Kechechyan,[18] D. Kettler,[50] D. P. Kikola,[22] J. Kiryluk,[22] A. Kisiel,[49] S. R. Klein,[22] A. G. Knospe,[53] A. Kocoloski,[23] D. D. Koetke,[47] T. Kollegger,[12] J. Konzer,[34] I. Koralt,[30] L. Koroleva,[16] W. Korsch,[20] L. Kotchenda,[26] V. Kouchpil,[11] P. Kravtsov,[26] K. Krueger,[1] M. Krus,[10] L. Kumar,[19] P. Kurnadi,[6] M. A. C. Lamont,[3] J. M. Landgraf,[3] S. LaPointe,[51] J. Lauret,[3] A. Lebedev,[3] R. Lednicky,[18] C.-H. Lee,[35] J. H. Lee,[3] W. Leight,[23] M. J. LeVine,[3] C. Li,[39] L. Li,[44] N. Li,[52] W. Li,[41] X. Li,[40] X. Li,[34] Y. Li,[45] Z. M. Li,[52] G. Lin,[53] S. J. Lindenbaum,[27,*] M. A. Lisa,[29] F. Liu,[52] H. Liu,[5] J. Liu,[37] T. Ljubicic,[3] W. J. Llope,[37] R. S. Longacre,[3] W. A. Love,[3] Y. Lu,[39] X. Luo,[39] G. L. Ma,[41] Y. G. Ma,[41] D. P. Mahapatra,[13] R. Majka,[53] O. I. Mall,[5] L. K. Mangotra,[17] R. Manweiler,[47] S. Margetis,[19] C. Markert,[44] H. Masui,[22] H. S. Matis,[22] Yu. A. Matulenko,[33] D. McDonald,[37] T. S. McShane,[9] A. Meschanin,[33] R. Milner,[23] N. G. Minaev,[33] S. Mioduszewski,[43] A. Mischke,[28] M. K. Mitrovski,[12] B. Mohanty,[48] M. M. Mondal,[48] B. Morozov,[16] D. A. Morozov,[33] M. G. Munhoz,[38] B. K. Nandi,[14] C. Nattrass,[53] T. K. Nayak,[48] J. M. Nelson,[2] P. K. Netrakanti,[34] M. J. Ng,[4] L. V. Nogach,[33] S. B. Nurushev,[33] G. Odyniec,[22] A. Ogawa,[3] V. Okorokov,[26] E. W. Oldag,[44] D. Olson,[22] M. Pachr,[10] B. S. Page,[15] S. K. Pal,[48] Y. Pandit,[19] Y. Panebratsev,[18] T. Pawlak,[49] T. Peitzmann,[28] V. Perevoztchikov,[3] C. Perkins,[4] W. Peryt,[49] S. C. Phatak,[13] P. Pile,[3] M. Planinic,[54] M. A. Ploskon,[22] J. Pluta,[49] D. Plyku,[30] N. Poljak,[54] A. M. Poskanzer,[22] B. V. K. S. Potukuchi,[17] C. B. Powell,[22] D. Prindle,[50] C. Pruneau,[51] N. K. Pruthi,[31] P. R. Pujahari,[14] J. Putschke,[53] R. Raniwala,[36] S. Raniwala,[36] R. L. Ray,[44] R. Redwine,[23] R. Reed,[5] H. G. Ritter,[22] J. B. Roberts,[37] O. V. Rogachevskiy,[18] J. L. Romero,[5] A. Rose,[22] C. Roy,[42] L. Ruan,[3] R. Sahoo,[42] S. Sakai,[6] I. Sakrejda,[22] T. Sakuma,[23] S. Salur,[5] J. Sandweiss,[53] E. Sangaline,[5] J. Schambach,[44] R. P. Scharenberg,[34] N. Schmitz,[24] T. R. Schuster,[12] J. Seele,[23] J. Seger,[9] I. Selyuzhenkov,[15] P. Seyboth,[24] E. Shahaliev,[18] M. Shao,[39] M. Sharma,[51] S. S. Shi,[52] E. P. Sichtermann,[22] F. Simon,[24] R. N. Singaraju,[48] M. J. Skoby,[34] N. Smirnov,[53] P. Sorensen,[3] J. Sowinski,[15] H. M. Spinka,[1] B. Srivastava,[34] T. D. S. Stanislaus,[47] D. Staszak,[6] J. R. Stevens,[15] R. Stock,[12] M. Strikhanov,[26] B. Stringfellow,[34] A. A. P. Suaide,[38] M. C. Suarez,[8] N. L. Subba,[19] M. Sumbera,[11] X. M. Sun,[22] Y. Sun,[39] Z. Sun,[21] B. Surrow,[23] D. N. Svirida,[16] T. J. M. Symons,[22] A. Szanto de Toledo,[38] J. Takahashi,[7] A. H. Tang,[3] Z. Tang,[39] L. H. Tarini,[51] T. Tarnowsky,[25] D. Thein,[44] J. H. Thomas,[22] J. Tian,[41] A. R. Timmins,[51] S. Timoshenko,[26] D. Tlusty,[11] M. Tokarev,[18] T. A. Trainor,[50] V. N. Tram,[22] S. Trentalange,[6] R. E. Tribble,[43] O. D. Tsai,[6] J. Ulery,[34] T. Ullrich,[3] D. G. Underwood,[1] G. Van Buren,[3] M. van Leeuwen,[28] G. van Nieuwenhuizen,[23] J. A. Vanfossen Jr.,[19] R. Varma,[14] G. M. S. Vasconcelos,[7] A. N. Vasiliev,[33] F. Videbaek,[3] Y. P. Viyogi,[48] S. Vokal,[18] S. A. Voloshin,[51] M. Wada,[44] M. Walker,[23] F. Wang,[34] G. Wang,[6] H. Wang,[25] J. S. Wang,[21] Q. Wang,[34] X. L. Wang,[39] Y. Wang,[45] G. Webb,[20] J. C. Webb,[3] G. D. Westfall,[25] C. Whitten Jr.,[6] H. Wieman,[22] S. W. Wissink,[15] R. Witt,[46] Y. F. Wu,[52] W. Xie,[34] N. Xu,[22] Q. H. Xu,[40] W. Xu,[6] Y. Xu,[39] Z. Xu,[3] L. Xue,[41] Y. Yang,[21] P. Yepes,[37] K. Yip,[3] I.-K. Yoo,[35] Q. Yue,[45] M. Zawisza,[49] H. Zbroszczyk,[49] W. Zhan,[21] J. B. Zhang,[52] S. Zhang,[41] W. M. Zhang,[19] X. P. Zhang,[22] Y. Zhang,[22] Z. P. Zhang,[39] J. Zhao,[41] C. Zhong,[41] J. Zhou,[37] W. Zhou,[40] X. Zhu,[45] Y. H. Zhu,[41] R. Zoulkarneev,[18] and Y. Zoulkarneeva[18]

(STAR Collaboration)

[1]*Argonne National Laboratory, Argonne, Illinois 60439, USA*

[2]*University of Birmingham, Birmingham, United Kingdom*

[3]*Brookhaven National Laboratory, Upton, New York 11973, USA*

[4]*University of California, Berkeley, California 94720, USA*

[5]*University of California, Davis, California 95616, USA*

[6]*University of California, Los Angeles, California 90095, USA*

[7]*Universidade Estadual de Campinas, Sao Paulo, Brazil*

[8]*University of Illinois at Chicago, Chicago, Illinois 60607, USA*

[9]*Creighton University, Omaha, Nebraska 68178, USA*
[10]*Czech Technical University in Prague, FNSPE, Prague, CZ-11519, Czech Republic*
[11]*Nuclear Physics Institute AS CR, 250 68 Řež/Prague, Czech Republic*
[12]*University of Frankfurt, Frankfurt, Germany*
[13]*Institute of Physics, Bhubaneswar 751005, India*
[14]*Indian Institute of Technology, Mumbai, India*
[15]*Indiana University, Bloomington, Indiana 47408, USA*
[16]*Alikhanov Institute for Theoretical and Experimental Physics, Moscow, Russia*
[17]*University of Jammu, Jammu 180001, India*
[18]*Joint Institute for Nuclear Research, Dubna, RU-141980, Russia*
[19]*Kent State University, Kent, Ohio 44242, USA*
[20]*University of Kentucky, Lexington, Kentucky, 40506-0055, USA*
[21]*Institute of Modern Physics, Lanzhou, China*
[22]*Lawrence Berkeley National Laboratory, Berkeley, California 94720, USA*
[23]*Massachusetts Institute of Technology, Cambridge, Massachusetts 02139-4307, USA*
[24]*Max-Planck-Institut für Physik, Munich, Germany*
[25]*Michigan State University, East Lansing, Michigan 48824, USA*
[26]*Moscow Engineering Physics Institute, Moscow, Russia*
[27]*City College of New York, New York City, New York 10031, USA*
[28]*NIKHEF and Utrecht University, Amsterdam, The Netherlands*
[29]*Ohio State University, Columbus, Ohio 43210, USA*
[30]*Old Dominion University, Norfolk, Virginia 23529, USA*
[31]*Panjab University, Chandigarh 160014, India*
[32]*Pennsylvania State University, University Park, Pennsylvania 16802, USA*
[33]*Institute of High Energy Physics, Protvino, Russia*
[34]*Purdue University, West Lafayette, Indiana 47907, USA*
[35]*Pusan National University, Pusan, Republic of Korea*
[36]*University of Rajasthan, Jaipur 302004, India*
[37]*Rice University, Houston, Texas 77251, USA*
[38]*Universidade de Sao Paulo, Sao Paulo, Brazil*
[39]*University of Science & Technology of China, Hefei 230026, China*
[40]*Shandong University, Jinan, Shandong 250100, China*
[41]*Shanghai Institute of Applied Physics, Shanghai 201800, China*
[42]*SUBATECH, Nantes, France*
[43]*Texas A&M University, College Station, Texas 77843, USA*
[44]*University of Texas, Austin, Texas 78712, USA*
[45]*Tsinghua University, Beijing 100084, China*
[46]*United States Naval Academy, Annapolis, Maryland 21402, USA*
[47]*Valparaiso University, Valparaiso, Indiana 46383, USA*
[48]*Variable Energy Cyclotron Centre, Kolkata 700064, India*
[49]*Warsaw University of Technology, Warsaw, Poland*
[50]*University of Washington, Seattle, Washington 98195, USA*
[51]*Wayne State University, Detroit, Michigan 48201, USA*
[52]*Institute of Particle Physics, CCNU (HZNU), Wuhan 430079, China*
[53]*Yale University, New Haven, Connecticut 06520, USA*
[54]*University of Zagreb, Zagreb, HR-10002, Croatia*

(Received 14 April 2010; published 30 August 2010)

Yields, correlation shapes, and mean transverse momenta p_T of charged particles associated with intermediate- to high-p_T trigger particles ($2.5 < p_T < 10$ GeV/c) in d + Au and Au + Au collisions at $\sqrt{s_{NN}} = 200$ GeV are presented. For associated particles at higher $p_T \gtrsim 2.5$ GeV/c, narrow correlation peaks are seen in d + Au and Au + Au, indicating that the main production mechanism is jet fragmentation. At lower associated particle $p_T < 2$ GeV/c, a large enhancement of the near- ($\Delta\phi \sim 0$) and away-side ($\Delta\phi \sim \pi$) associated yields is found, together with a strong broadening of the away-side azimuthal distributions in Au + Au collisions compared to d + Au measurements, suggesting that other particle production mechanisms play a role. This is further supported by the observed significant softening of the away-side associated particle yield distribution at $\Delta\phi \sim \pi$ in central Au + Au collisions.

DOI: 10.1103/PhysRevC.82.024912 PACS number(s): 25.75.Nq, 25.75.Bh

I. INTRODUCTION

The goal of ultrarelativistic heavy-ion collisions is to create a system of deconfined quarks and gluons at high temperature and density and study its properties. In the initial stage of the collision, hard scatterings between partons in the incoming nuclei produce high transverse momentum (p_T) partons that fragment into jets of hadrons with a clear back-to-back di-jet signature [1]. In Au + Au collisions, hard partons traverse the hot and dense colored medium, thus probing the medium through energy loss [2–4].

In-medium jet energy loss was first observed at the BNL Relativistic Heavy Ion Collider (RHIC) as a suppression of hadron spectra at high p_T [5,6] in Au + Au collisions with respect to p + p collisions. The jetlike structure of hadron production at high p_T was confirmed by measurements of the azimuthal angle difference $\Delta\phi$ distributions of *associated* particles in a certain range of p_T with respect to a *trigger* hadron at a higher p_T [1]. At the highest p_T, a suppression of the away-side yield (around $\Delta\phi \sim \pi$ with respect to the trigger particle) by a factor 3–5 is observed [7]. This suppression is consistent with theoretical calculations that incorporate in-medium energy loss [8,9]. At lower p_T of the associated particles, a strongly broadened away-side structure is seen in Au + Au collisions, and the associated yields on both the near-side ($\Delta\phi \sim 0$) and away-side ($\Delta\phi \sim \pi$) are enhanced [10,11]. A number of possible explanations of the away-side broadening at intermediate p_T have been put forward, ranging from fragmentation products of radiated gluons [12,13] to medium response and the possibility of a Mach-cone shock wave [14–17].

The $p_T^{\rm trig}$ range used in previous studies [10,11] is the region where the p/π ratio is large. The large baryon/meson ratio has been interpreted as being due to coalescence and recombination of quarks, which could also have an impact on the jetlike correlation yields, especially for trigger particles in the p_T range 2.0 to 4.0 GeV/c where coalescence and recombination products [18–20] may be present.

In this paper, we present a systematic exploration of the azimuthal di-hadron correlation shapes and yields with centrality and p_T of the trigger ($p_T^{\rm trig}$) and associated hadrons ($p_T^{\rm assoc}$), to investigate the change from broadened correlation peaks with enhanced yields at low p_T to suppressed away-side yields at high p_T. The analysis is performed on the large statistics sample of Au + Au collisions at $\sqrt{s_{NN}} =$ 200 GeV collected by the STAR experiment in the RHIC run in 2004. The d + Au data sample from the year 2003 is used as a reference where no hot and dense matter is formed, because the minimum-bias p + p data collected by STAR has limited statistics. Earlier studies have shown that di-hadron correlations in p + p and d + Au collisions are similar [1].

II. EXPERIMENTAL SETUP AND DATA SETS

The measurements presented in this paper were performed with the solenoidal tracker at RHIC (STAR) detector [21]. Charged tracks are reconstructed with the time projection chamber (TPC) [22].

For Au + Au collisions, two different online event selections (triggers), minimum-bias and central, were used. The central trigger selection was based on the energy deposited in the two zero-degree calorimeters (ZDCs) which measure spectator fragments and small-angle particle production [21]. The trigger selected the most central 12% of the total hadronic cross section, based on a maximum energy deposited in the ZDCs and a minimum multiplicity in the central trigger barrel (CTB) [23]. The central trigger also uses time information from the beam-beam counters (BBCs) to restrict the primary vertex position $z_{\rm vtx}$ to be within approximately ±30 cm of the center of the detector along the beam direction. The minimum-bias (MB) trigger is based on a ZDC coincidence (a threshold amount of energy in each ZDC) and requires a minimum multiplicity in the CTB to reject nonhadronic interactions. For the minimum-bias sample, events were selected to have $|z_{\rm vtx}| < 25$ cm. A total of 21×10^6 minimum-bias events and 18×10^6 central triggered Au + Au events were used.

For d + Au collisions, the MB trigger was defined by requiring that at least one beam-rapidity neutron impinge on the ZDC in the Au beam direction. The measured MB cross section amounts to $95 \pm 3\%$ of the total d + Au geometric cross section [1]. For d + Au events, the distribution of primary vertices along the beamline was wider than during the Au + Au run. The events were selected to be within ±50 cm from the center of the detector along the beamline. A total of 3.4×10^6 d + Au events were selected for this analysis.

The Au + Au events are further divided into centrality classes based on the uncorrected charged-particle multiplicity in the range $|\eta| < 0.5$ as measured by the TPC. We present results for the following centrality ranges: 0–12% (from the central triggered data set), 20–40%, 40–60%, and 60–80% (from the MB data set) of the total hadronic cross section, with 0% referring to the most central collisions.

III. DATA ANALYSIS

Di-hadron correlations are constructed using charged particles measured in the TPC. All particles are selected to have pseudorapidity in the range $-1.0 < \eta < 1.0$, so that they fall well within the TPC acceptance. To reject background tracks at high p_T, tracks were required to have at least 20 measured points in the TPC (out of 45) and a distance of closest approach (dca) to the event vertex of less than 1 cm to reduce the contribution from secondary particles.

The results are corrected for single-particle acceptance and detection efficiency as well as for the pair acceptance as a function of $\Delta\phi$. The single-particle reconstruction efficiency as a function of η, p_T, and centrality is determined using hits from a Monte Carlo simulation which are embedded into real data events. The tracking efficiency depends sensitively on the gain in the proportional readout chamber of the TPC and thus on the atmospheric pressure. Uncertainties in the details of these effects give rise to an overall 5% systematic uncertainty in the absolute yields given in this paper. In most cases, the uncertainty from the background subtraction as described in

*Deceased.

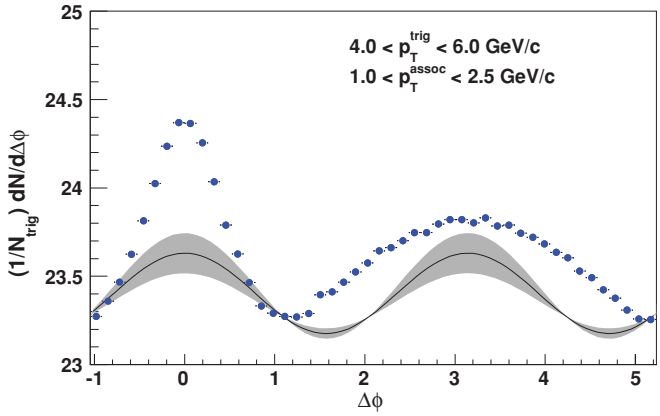

FIG. 1. (Color online) Azimuthal distribution of associated charged particles with $1.0 < p_T^{\rm assoc} < 2.5$ GeV/c with respect to trigger particles with $4.0 < p_T^{\rm trig} < 6.0$ GeV/c in 0–12% central Au + Au collisions. The curve shows the modulation of the background due to elliptic flow v_2, and the grey band indicates the uncertainty on the elliptic flow of the background (see text).

the next section is larger than the systematic uncertainty from the tracking efficiency. The TPC sector boundaries introduce a dependence of the pair acceptance on angle difference $\Delta\phi$, which was determined from mixed events. No $\Delta\eta$ pair acceptance correction has been applied. A small inefficiency due to tracks crossing inside the TPC volume affects the associated hadron distribution at small pair separation in $(\Delta\eta, \Delta\phi)$. This effect manifests itself as a reduced efficiency for small but finite $\Delta\phi$, at positive or negative $\Delta\phi$, depending on the sign of the curvature of the associate track. A correction was performed by first curvature-sorting the distributions and then reflecting a few bins from the unaffected area to the area where the inefficiency occurs, thus restoring the symmetry between positive and negative $\Delta\phi$.

Figure 1 shows an example azimuthal angle difference distribution for trigger particles with $4.0 < p_T^{\rm trig} < 6.0$ GeV/c and associated particles with $1.0 < p_T^{\rm assoc} < 2.5$ GeV/c in 0–12% central Au + Au collisions. The distribution is divided by the number of trigger hadrons to give the associated yield per trigger hadron. The associated hadron distribution contains a background of uncorrelated particles which has a $\cos(2\Delta\phi)$ modulation due to the correlation of all particles with the reaction plane through elliptic flow v_2. We model the background using the function $B[1 + 2\langle v_2^{\rm trig}\rangle\langle v_2^{\rm assoc}\rangle \cos(2\Delta\phi)]$, where the v_2 values are from separate flow measurements [24]. The function is normalized to the data in the region $0.8 < |\Delta\phi| < 1.2$, where the signal is apparently small, and then subtracted. This background normalization procedure is often referred to as the ZYA1 (zero yield at 1 radian) or ZYAM (zero yield at minimum) method [25].

The method of normalizing the combinatorial background level in the region around $|\Delta\phi| = 1$ was first used for di-hadron correlations at higher momenta [7,10], where there are narrow peaks on the near and away sides, separated by a largely "signal-free" region. At lower p_T, the correlation peaks are broader, and there is no clear signal-free region, so the background normalization is more ambiguous. In addition, because of the larger combinatorial background, the elliptic flow modulation of the background is of similar size as the trigger-associated-hadron correlation signal. The ZYA1 method provides a simple prescription to separate signal and background, which we will use throughout the paper. An alternative approach would be to decompose the correlation shape using a fit function with components representing the flow modulation of the background and the assumed shapes of near- and away-side correlation peaks [26,27]. The unsubtracted azimuthal hadron distributions are provided in the Appendix and can be used for such a procedure.

The nominal v_2 value used for the subtraction is the mean of the v_2 measured using the reaction plane method with the forward TPC and the four-particle cumulant method, which have different sensitivity to nonflow effects and flow fluctuations [24] (line in Fig. 1). The difference between the two results is used as the estimate of the systematic uncertainty in v_2, and this range is shown by the band in Fig. 1. For the d + Au results, a constant pedestal (normalized in the same $\Delta\phi$ range) was subtracted.

IV. RESULTS

A. Azimuthal di-hadron distributions

Figure 2 shows the background-subtracted associated hadron $\Delta\phi$ distributions with $1.0 < p_T^{\rm assoc} < 2.5$ GeV/c for four centrality selections, 60–80%, 40–60%, 20–40% and 0–12%, and four trigger selections, $2.5 < p_T^{\rm trig} < 3.0$, $3.0 < p_T^{\rm trig} < 4.0$, $4.0 < p_T^{\rm trig} < 6.0$, and $6.0 < p_T^{\rm trig} < 10.0$ GeV/c. Results are presented for two different ranges in the pseudorapidity difference between the trigger and associated particles $|\Delta\eta|$. The shapes are very similar for both $\Delta\eta$ selections in all panels (there is an overall reduction in the away-side yields due to the smaller acceptance for $|\Delta\eta| < 0.7$). For reference, the di-hadron distributions without background subtraction are shown in the Appendix, where also the v_2 values and background normalization values (B) used to subtract the background are given. The systematic uncertainties on the v_2 values for the background are shown by the bands around the data points. The d + Au results (open circles) are also shown for reference.

In Fig. 2, top row, one observes that the jetlike correlations in peripheral (60–80% centrality) Au + Au collisions are very similar to the d + Au result, indicating that such correlations in peripheral Au + Au collisions can be described as a superposition of independent $p + p$ collisions. The near- and away-side yields of associated particles increase with $p_T^{\rm trig}$, as expected from parton fragmentation.

For more central events, a significant increase of both the near- and the away-side yields is seen in Au + Au collisions relative to d + Au. The relative increase of the near-side yield is larger for lower $p_T^{\rm trig}$ (top row) than for higher $p_T^{\rm trig}$. For peripheral events, the near-side results for $|\Delta\eta| < 0.7$ do not differ significantly from the full acceptance results, demonstrating that the correlated yield is at relatively small $\Delta\eta$, as expected from jet fragmentation. For more central collisions, on the other hand, a significant fraction of the

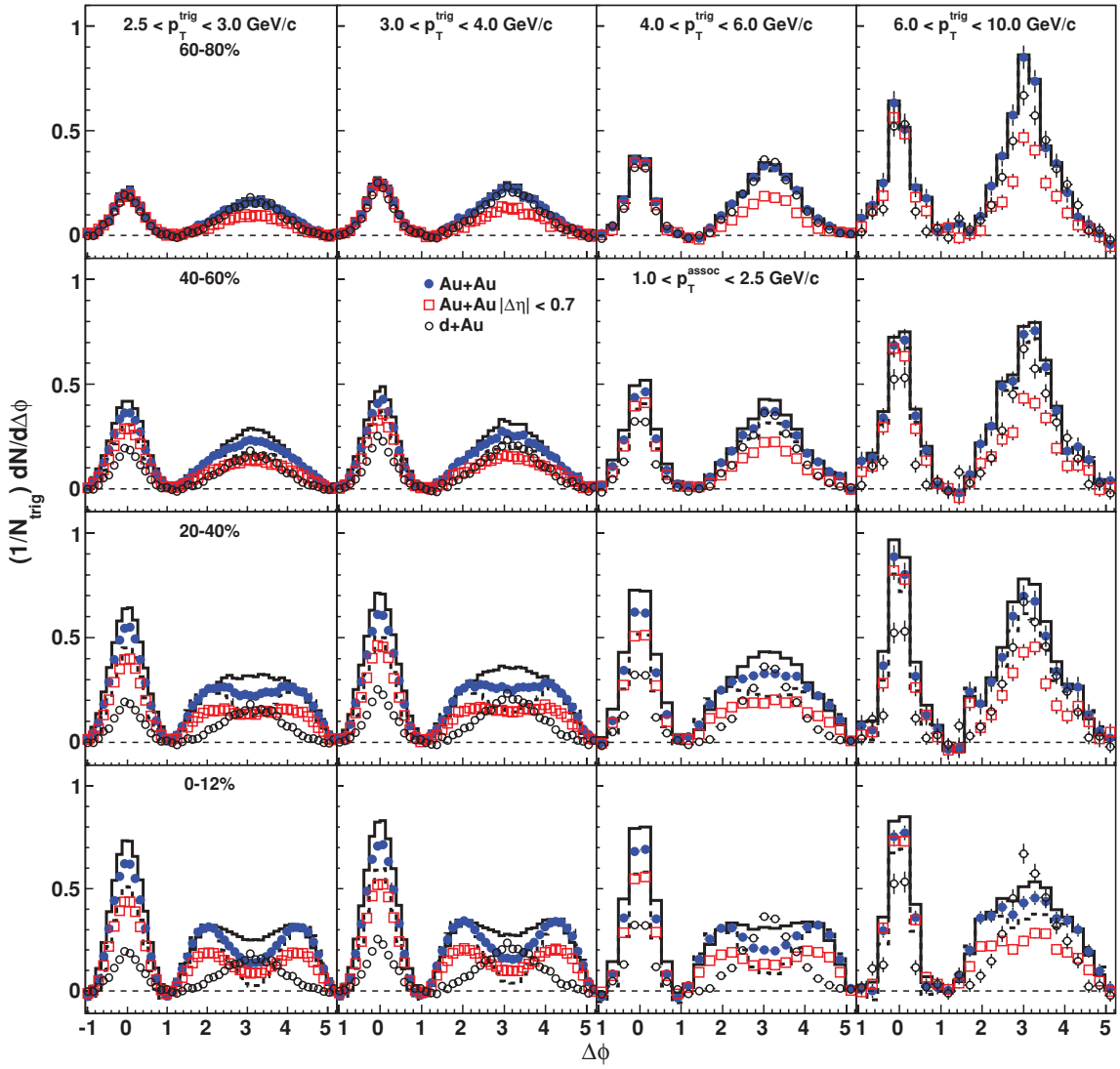

FIG. 2. (Color online) Background-subtracted azimuthal angle difference distributions for associated particles with p_T between 1.0 and 2.5 GeV/c and for different ranges of trigger particle p_T, ranging from 2.5–3.0 GeV/c (left column) to 6–10 GeV/c (right column). Results are shown for Au + Au collisions (solid circles) with different centrality (rows) and d + Au reference results (open circles). The rapidity range is $|\eta| < 1$ and as a result the rapidity difference $|\Delta\eta| < 2$. Open red squares show results for a restricted acceptance of $|\Delta\eta| < 0.7$, using tracks within $|\eta| < 1$. The solid and dashed histograms show the upper and lower range of the systematic uncertainty due to the v_2 modulation of the subtracted background.

associated yield is at large $|\Delta\eta| > 0.7$ for the lower p_T^{trig}, indicating a significant long-range correlation in $\Delta\eta$, possibly due to an interplay between the soft bulk dynamics of longitudinal flow and jetlike di-hadron structure [28]. It has also been argued recently that this long-range correlation in $\Delta\eta$ could be caused by long-range structures in the medium, due to density fluctuations in the medium [29] or color flux tubes [30–32]. The "ridge"-like correlation structure in $\Delta\eta$ is further explored in other STAR publications [26,33–35].

It is interesting to note that the largest relative enhancement of the near-side yield is observed for the lower p_T^{trig}, 2.5–4.0 GeV/c. It has been suggested that particle production in this momentum range has a large contribution from coalescence of quarks from bulk partonic matter [18–20]. This production mechanism would not lead to jetlike structures. Trigger hadrons formed by this mechanism would increase the number of trigger hadrons, without increasing the associated yield, leading to a reduced per-trigger associated yield, in contrast to what is observed in Fig. 2. The increased associated yield at intermediate p_T indicates that if coalescence is a significant source of hadron production at intermediate p_T, it has to generate an angular correlation structure, either through shower-thermal coalescence [36] or local fluctuations in the medium density or temperature, e.g., due to heating of the medium by the passage of a parton [37]. So far, most calculations of such effects are qualitative at best. Quantitative predictions for these processes should be made and compared with the data. Measurements with identified baryons and mesons as trigger and associated particles [38,39] can be used to explore the possible contributions from coalescence.

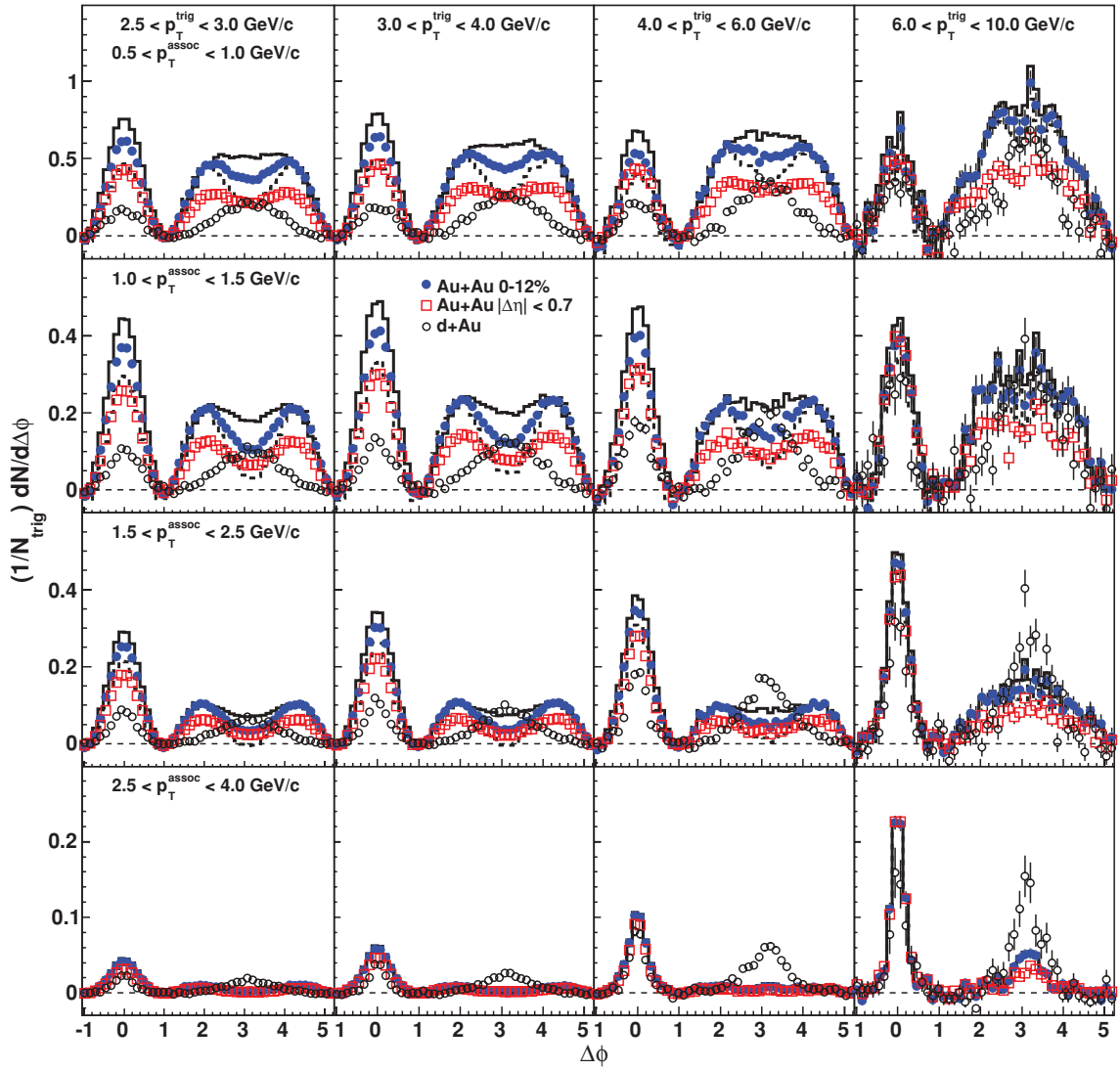

FIG. 3. (Color online) Background-subtracted azimuthal angle difference distributions for different $p_T^{\rm trig}$ (columns) and $p_T^{\rm assoc}$ (rows) in 0–12% central Au + Au collisions (solid circles) and d + Au reference results (open circles). The rapidity range is $|\eta| < 1$ and as a result the rapidity difference $|\Delta\eta| < 2$. Open red squares show results for a restricted acceptance of $|\Delta\eta| < 0.7$, using tracks with $|\eta| < 1$. The solid and dashed histograms show the upper and lower range of the systematic uncertainty due to the v_2 modulation of the subtracted background.

The away-side yield of associated particles at low $p_T^{\rm trig}$ (top row, Fig. 2) evolves significantly in both shape and yield with centrality: the shape becomes much broader than the d + Au reference and the yield increases. For 20–40% central collisions, the distribution becomes flat or slightly double-peaked, with a shallow minimum at $\Delta\phi = \pi$. In the most central collisions, the distribution is double-peaked for the lowest $p_T^{\rm trig}$. With increasing $p_T^{\rm trig}$, the away-side shape becomes flatter. Overall, there is a smooth evolution of the peak shape with centrality and $p_T^{\rm trig}$. The value of $p_T^{\rm trig}$ for which the away side becomes flat or double-peaked decreases with centrality. Note that the double-peak shape is not seen in the raw signal in Fig. 1 and only appears after the subtraction of the v_2-modulated background. In that sense, the double-peak structure is generated by imposing a separation between flow and nonflow in the analysis of azimuthal correlations. This separation is not unambiguous and remains under active investigation.

For the most central collisions, the broadening of the away-side structure is so large that the near- and away-side peaks may overlap, making it impossible to unambiguously distinguish the correlation structure from the background without other inputs. For the present analysis, we have chosen to use the same background normalization procedure for all centrality bins and p_T bins, i.e., to normalize the v_2-modulated background to the signal in the range $0.8 < |\Delta\phi| < 1.2$ and subtract it.

In Fig. 3 we focus on central data where the largest modifications of the correlation shapes and yields are found. The figure shows the correlation shapes in the 0–12% central event sample for different selections of $p_T^{\rm assoc}$ and $p_T^{\rm trig}$. As in Fig. 2, results are given for the full $\Delta\eta$ acceptance (solid circles) as well as a restricted range $|\Delta\eta| < 0.7$ (squares), and for d + Au collisions (open circles). The distributions before background subtractions and the background normalization and v_2 values are given in the Appendix.

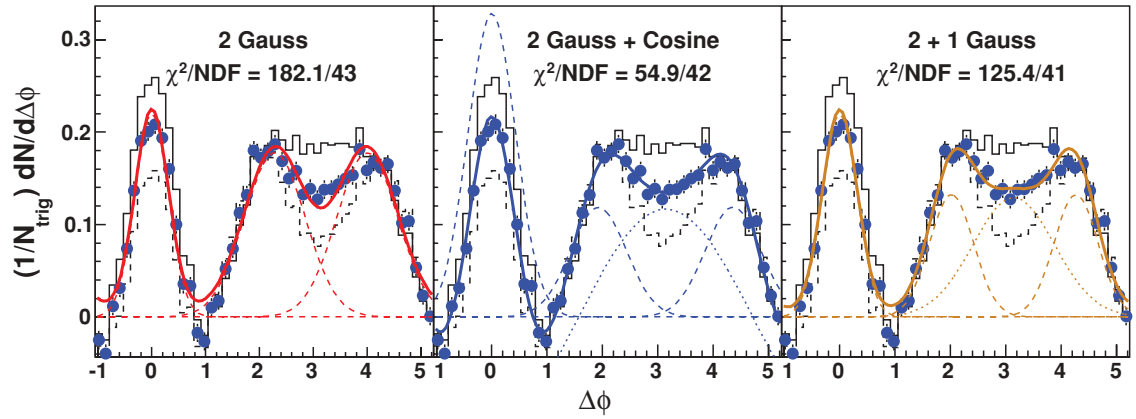

FIG. 4. (Color online) Background-subtracted associated hadron distribution in 0–12% central Au + Au collisions with $0.8 < p_T^{\rm assoc} < 1.0$ and $4 < p_T^{\rm trig} < 6$ GeV/c. The colored curves indicate fits with three different functional forms for the away-side shape: (left panel) symmetric identical Gaussian distributions (2 Gauss), (middle panel) adding a cos$\Delta\phi$ background distribution (2 Gauss + Cosine), and (right panel) adding a third Gaussian as the away-side jetlike component (2 + 1 Gauss). The histograms indicate the uncertainty on the background shape due to elliptic flow.

On the near side, we observe again a large increase of the yield in central Au + Au collisions compared to d + Au collisions. The yield depends on the $\Delta\eta$ selection used, indicating that there is significant associated yield at $\Delta\eta > 0.7$. The relative size of the enhancement depends on $p_T^{\rm assoc}$ and $p_T^{\rm trig}$. The measured jetlike yield in d + Au collisions increases faster with $p_T^{\rm trig}$ (going from left to right in Fig. 3) than in Au + Au collisions, reducing the relative size of the enhancement in Au + Au. The associated yield decreases with increasing $p_T^{\rm assoc}$ for both d + Au and Au + Au collisions, but the decrease is stronger in Au + Au, so the measured yields in Au + Au approach the d + Au results at the highest $p_T^{\rm assoc}$. A summary of the yields is presented in Fig. 6 (Sec. IV C).

On the away side, we observe a broadening and enhancement of the yield in Au + Au compared to d + Au, except at $2.5 < p_T^{\rm assoc} < 4.0$ GeV/c (bottom row of Fig. 3), where a broadening is seen, while the yield is smaller than in d + Au. For $6 < p_T^{\rm trig} < 10$ GeV/c (right-most column in Fig. 3), a narrow peak appears at large $p_T^{\rm assoc}$ in Au + Au, similar to what is seen in d + Au collisions and at higher p_T in Au + Au collisions [7].

Although the shape of the away-side distribution changes with $p_T^{\rm trig}$ and $p_T^{\rm assoc}$, there seems to be no gradual broadening as a function of p_T: the rising flanks of the away-side distribution are at similar $\Delta\phi$ in the entire range $0.5 < p_T^{\rm assoc} < 2.5$ GeV/c and $2.5 < p_T^{\rm trig} < 6$. In fact, it could be argued that the away-side distribution is as broad as possible; there is no $\Delta\phi$ region without a correlation signal.

The broad away-side correlation structure in Au + Au collisions is a truly remarkable observation. Although some broadening of the away-side correlation in Au + Au collisions would be expected due to increased acoplanarity (k_T) due to multiple scattering of the parton in the medium, the structures seen in Fig. 3 are broader than would be expected from such a mechanism [12]. It has, however, been pointed out that kinematic selection effects on in-medium gluon radiation may lead to a nontrivial structure in the angular distributions [13]. It has also been argued that a fast parton may generate sound waves in the bulk quark-gluon matter, which would lead to a Mach-cone shock wave [14–17]. Evidence for a conical emission pattern has been found in three-particle correlation measurements [40]. The broad structure seen in the di-hadron distribution could then be the projection of the conical pattern on $\Delta\phi$. Another mechanism that may produce conical emission from a fast parton is QCD Cherenkov radiation [41,42]. There are two other calculations that show a broad, double-peaked away-side structure without implementing a specific mechanism for conical emission: one is a three-dimensional hydrodynamical calculation which includes local density fluctuations in the initial state [29] and the other is the AMPT model [43]. It is worth noting that in

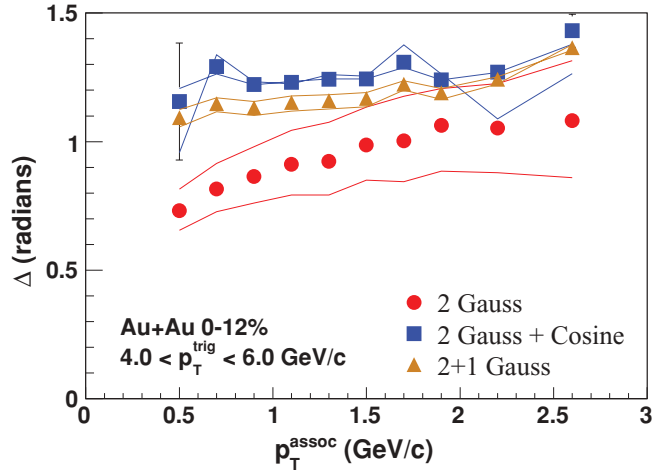

FIG. 5. (Color online) Angle Δ between the away-side peaks and $\Delta\phi = \pi$ for $4 < p_T^{\rm trig} < 6$ GeV/c in 0–12% central Au + Au collisions as a function of $p_T^{\rm assoc}$. Three different parametrizations of the away-side peak shape were used (see text). The lines show the systematic uncertainty from v_2 variation, while the errors are statistical errors from the fit.

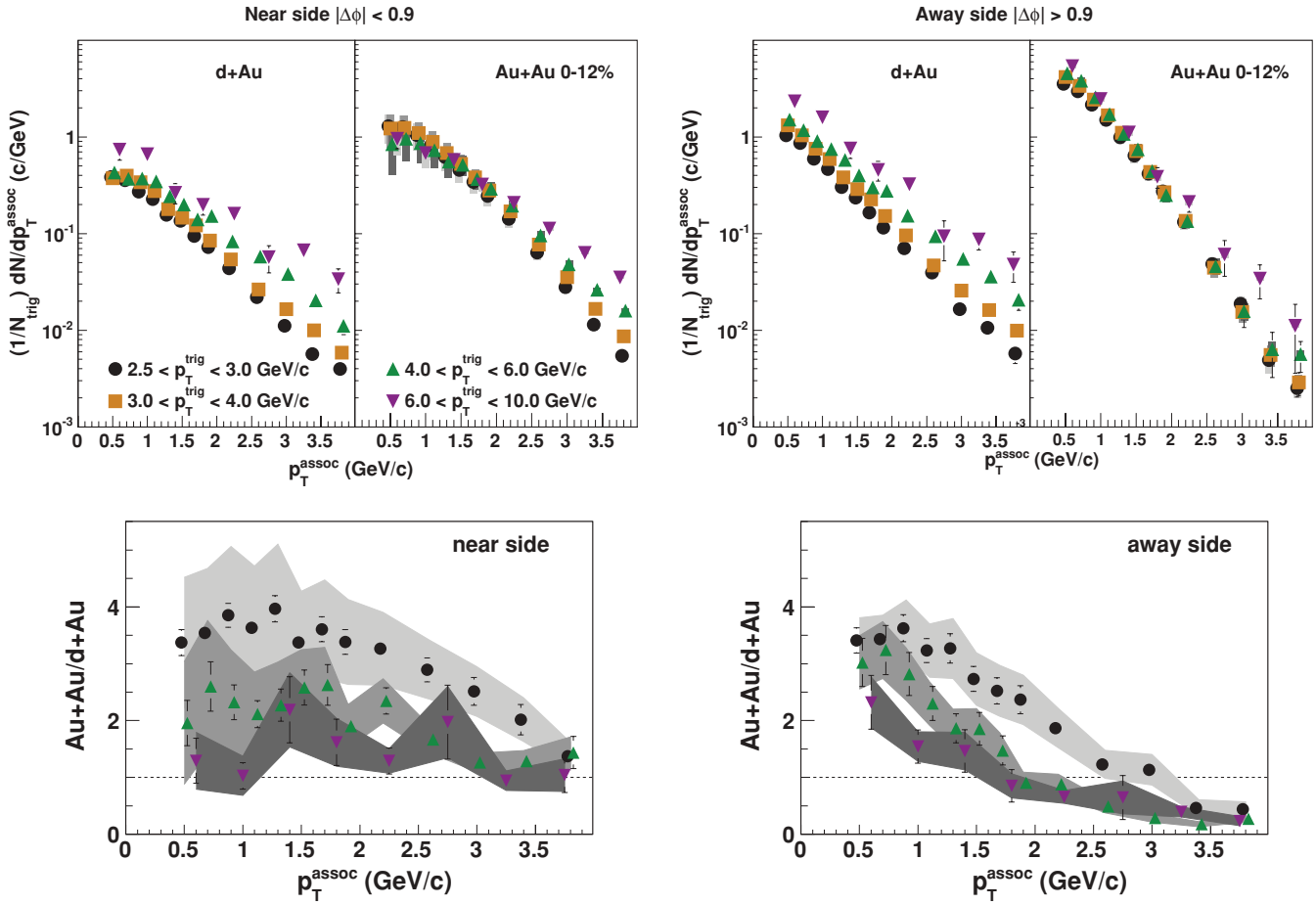

FIG. 6. (Color online) Near-side ($|\Delta\phi| < 0.9$, left panels) and away-side ($|\Delta\phi| > 0.9$, right panels) associated yield per trigger particle for various $p_T^{\rm trig}$ selections as a function of $p_T^{\rm assoc}$. Results are shown for 0–12% central Au + Au collisions and for d + Au collisions. The bottom panels show the ratios of the per-trigger associated yields in central Au + Au and d + Au collisions. The error bars on the points indicate the statistical uncertainty, including the statistical uncertainty on the subtracted background level. The gray bands indicate the uncertainty from the elliptic flow modulation of the background.

the three-dimensional hydrodynamical model, there is also no explicit introduction of hard partons or jets; the correlation arises purely from the medium. All these models should be confronted with the data presented in Figs. 2 and 3 as well as the three-particle correlation data in Ref. [40].

In addition to the change of the correlation shapes, a significant increase of the yields is seen in Au + Au collisions relative to d + Au collisions, for most of the p_T selections in Fig. 3, on both the near and the away sides. The yield increase implies that trigger hadrons in Au + Au collisions are accompanied by a larger energy flow than trigger hadrons with the same transverse momentum in elementary collisions. This would be compatible with a scenario where the leading hadron is softened due to energy loss so that trigger hadrons in Au + Au collisions select a larger initial parton energy than in d + Au or $p + p$ collisions.

B. Away-side shapes

To further characterize the broad shape of the away-side associated hadron distributions in Figs. 2 and 3, the data were fitted with different parametrizations. Three different functional forms were used, all of which are based on the assumption that there is significant yield in a cone in $(\Delta\eta,\Delta\phi)$ around the away-side parton. The projection of this cone on $\Delta\phi$ would give rise to two peaks symmetric around $\Delta\phi = \pi$. Figure 4 shows the associated hadron distribution after background subtraction for $4 < p_T^{\rm trig} < 6$ GeV/c and $0.8 < p_T^{\rm assoc} < 1.0$ GeV/c fitted with three different functional forms that include two Gaussian distributions at $\Delta\phi = \pi \pm \Delta$ on the away side. The left panel of Fig. 4 shows the simplest ansatz, using just two Gaussian peaks on the away side and a single Gaussian peak on the near side. To account for correlations induced by momentum conservation or remnant jet structure, we add a $\cos(\Delta\phi)$ distribution (middle panel of Fig. 4) or a third Gaussian peak (with a different width and amplitude) at $\Delta\phi = \pi$ (right panel Fig. 4). The three parametrizations are referred to as 2 Gauss, 2 Gauss + Cosine and 2 + 1 Gauss, respectively. The best fit is obtained when using the 2 Gauss + Cosine function, as can be seen from the χ^2 values given in the figure.

Figure 5 shows Δ, the angle (in radians) between the Gaussian peaks and $\Delta\phi = \pi$, as a function of $p_T^{\rm assoc}$, for the

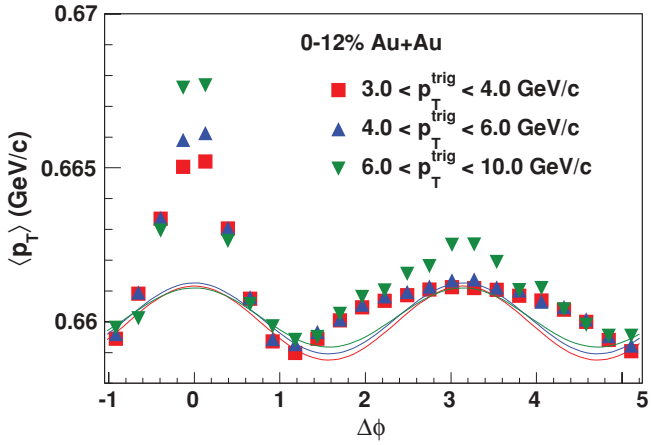

FIG. 7. (Color online) Inclusive, azimuthal $\langle p_T \rangle$ of associated hadrons between 0.25 and 4.0 GeV/c in all events containing various classes of trigger particles. The lines show the v_2-modulated background for the different trigger ranges, with the colors corresponding to the data points.

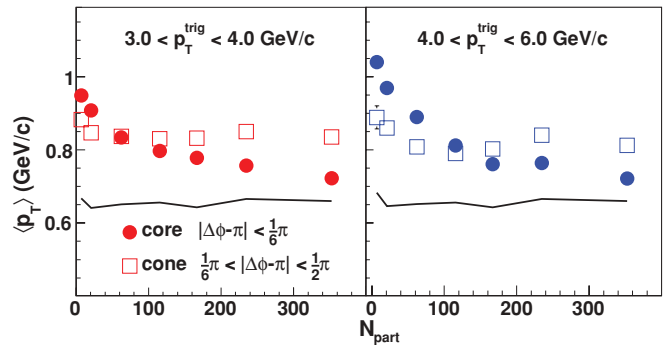

FIG. 9. (Color online) Mean transverse momentum $\langle p_T \rangle(\Delta\phi)$ of associated hadrons in the range $0.25 < p_T^{\rm assoc} < 4.0$ GeV/c in the core ($|\Delta\phi - \pi| < \frac{\pi}{6}$) and cone ($\frac{\pi}{6} < |\Delta\phi - \pi| < \frac{\pi}{2}$) azimuthal regions for $3 < p_T^{\rm trig} < 4$ and $4 < p_T^{\rm trig} < 6$ GeV/c as a function of number of participants. The lines indicate the inclusive $\langle p_T \rangle$ in the same p_T range for events with a trigger hadron.

three different parametrizations of the away-side shape for $4 < p_T^{\rm trig} < 6$ GeV/c in the 0–12% most central collisions. Similar results were obtained for $3 < p_T^{\rm trig} < 4$ GeV/c (not shown).

The peak positions Δ in Fig. 5 show a slow increase with $p_T^{\rm assoc}$ for the fits with the symmetric Gaussian form. This functional form alone, however, does not provide a good description of the away-side shape for larger $p_T^{\rm trig}$ and $p_T^{\rm assoc}$. When an away-side contribution at $\Delta\phi = \pi$ is included (2 + 1 Gauss and and 2 Gauss+Cosine shapes), the peak position Δ is close to 1.2 and approximately independent of $p_T^{\rm assoc}$. This observation is qualitatively consistent with predictions for a Mach cone developing in the hot and dense medium of the early stage of the collision [15] and with existing results on three-particle azimuthal correlations [40].

C. Associated particle spectra

Figure 6 shows the integrated yield in the near-side peak ($|\Delta\phi| < 0.9$) and away-side ($|\Delta\phi| > 0.9$) as a function of $p_T^{\rm assoc}$ in central Au + Au collisions and d + Au collisions for four $p_T^{\rm trig}$ intervals. The lower panels of the figures show the ratio of the associated yields in central Au + Au collisions and d + Au collisions.

For d + Au collisions, the associated yield clearly increases with increasing $p_T^{\rm trig}$ and the slope decreases with $p_T^{\rm trig}$. These trends are expected from parton fragmentation, where the larger $p_T^{\rm trig}$ selects larger underlying parton energies, thus increasing the multiplicity in the jet and leading to a harder fragmentation.

The lower panels of Fig. 6 show that the ratio of the yields in Au + Au and d + Au is decreasing with $p_T^{\rm assoc}$, indicating that the fragmentation is softened due to in-medium energy loss. A softer fragmentation also implies that a trigger particle of given momentum selects different parton energies in Au + Au collisions than in d + Au collisions, which could explain

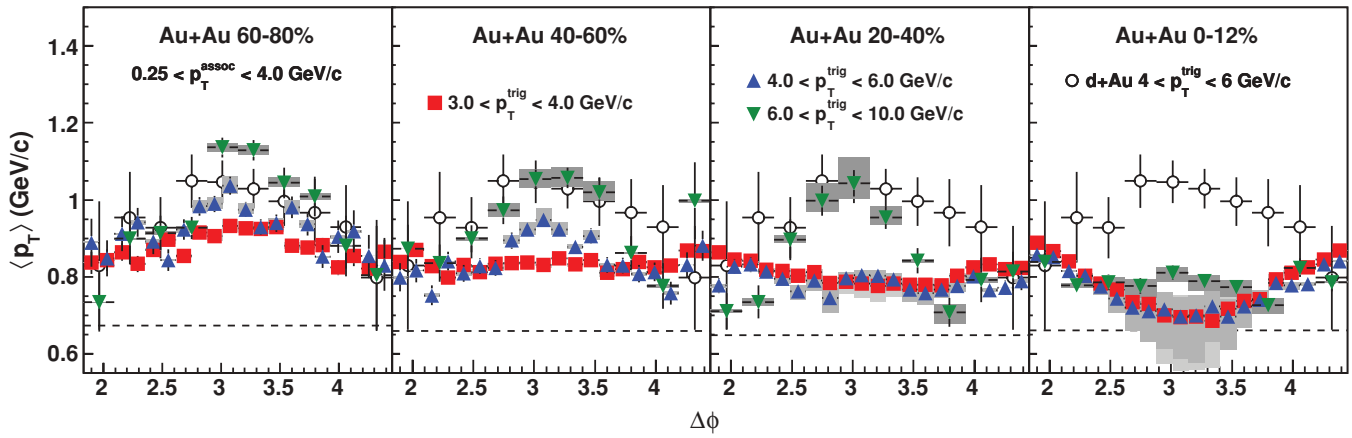

FIG. 8. (Color online) Mean transverse momentum $\langle p_T \rangle$ of associated particles with $0.25 < p_T^{\rm assoc} < 4.0$ GeV/c, for four different centrality selections. The shaded bands show the systematic uncertainty due to elliptic flow of the uncorrelated background. The dashed lines indicate the inclusive $\langle p_T \rangle$ in the same p_T range in events with a trigger particle.

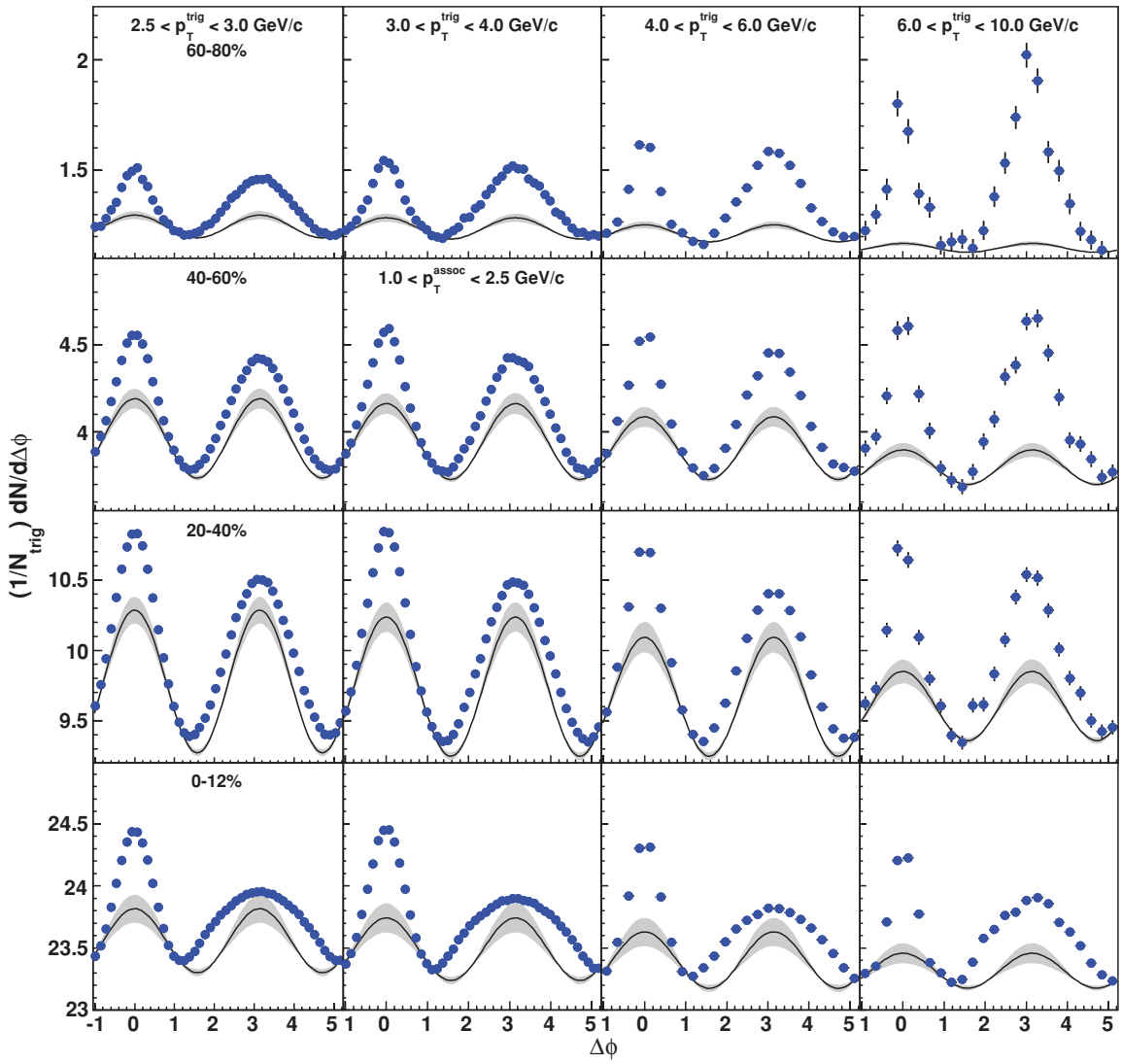

FIG. 10. (Color online) Azimuthal angle difference distributions for associated particles with p_T between 1.0 and 2.5 GeV/c and for different ranges of trigger particle p_T, ranging from 2.5–3.0 GeV/c (left column) to 6–10 GeV/c (right column). Results are shown for Au + Au collisions with different centrality (rows). The line and the grey band show the elliptic flow modulated background that was subtracted to obtain Fig. 2.

some of the enhancement of associated yield at lower p_T^{assoc} in Au + Au collisions. However, it should be noted that a large part of the increased yield at lower p_T^{assoc} is at large $\Delta\eta$, associated with the ridge effect, and is therefore not necessarily from jet fragments [34]. It is also possible that other sources of particle production, such as parton coalescence and resonance decays, contribute at lower p_T^{trig} and may lead to different behavior in d + Au and Au + Au.

D. Azimuthal angle dependent mean p_T

To further characterize the p_T dependence of associated particle production, we perform an analysis of the inclusive mean p_T, $\langle p_T\rangle$, of associated particles as a function of $\Delta\phi$. The azimuthal distribution $\langle p_T\rangle(\Delta\phi)$ is calculated by taking the ratio of the p_T-sum distribution $P_T(\Delta\phi)$ and the number distribution $N(\Delta\phi)$

$$\langle p_T\rangle(\Delta\phi) = P_T(\Delta\phi)/N(\Delta\phi). \tag{1}$$

The number distribution $N(\Delta\phi) = (1/N_{\text{trig}})dN/d\Delta\phi$, as shown in Fig. 1, while the p_T-sum distribution $P_T(\Delta\phi)$ is formed using the same procedure, but adding the (scalar) transverse momenta as weights in the azimuthal distribution.

To illustrate this method, Fig. 7 shows the inclusive distribution $\langle p_T\rangle(\Delta\phi)$ for $0.25 < p_T^{\text{assoc}} < 4.0$ GeV/c and three different p_T^{trig} selections for 0–12% central collisions. On the near side, a clear increase of $\langle p_T\rangle$ with p_T^{trig} is visible, while the away-side $\langle p_T\rangle$ distributions show a smaller dependence on p_T^{trig}. The lines in Fig. 7 show the background. The elliptic flow of the background is calculated as a weighted average of $v_2^{\text{trig}}v_2^{\text{assoc}}$. The difference between the p_T-weighted average $\langle v_2\rangle_{p_T}$, which is used to subtract the background in

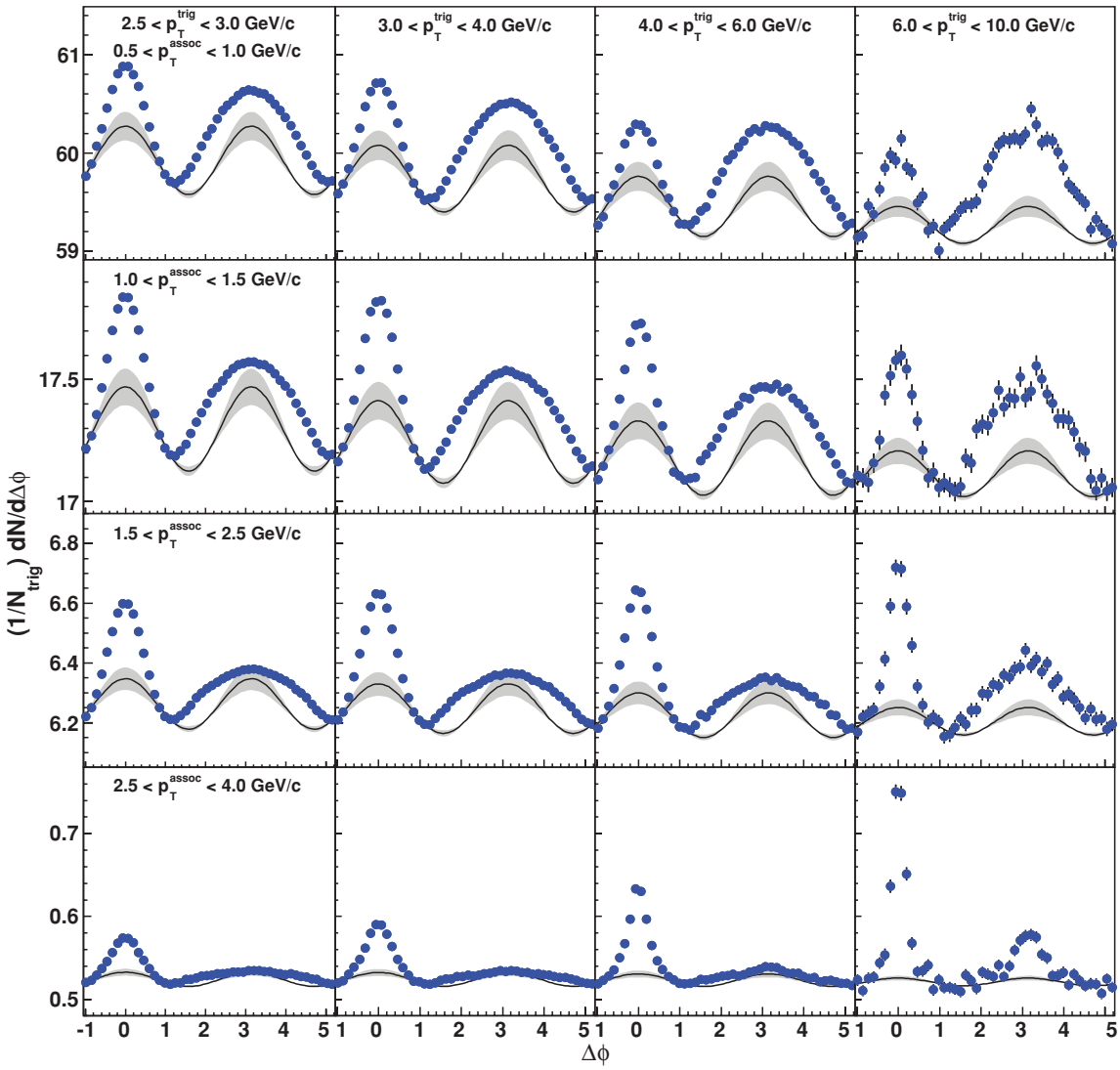

FIG. 11. (Color online) Azimuthal angle difference distributions for different $p_T^{\rm trig}$ (columns) and $p_T^{\rm assoc}$ (rows) in 0–12% central Au + Au collisions. The line and the grey band show the elliptic flow modulated background that was subtracted to obtain Fig. 3.

the p_T-weighted distribution, and the number-weighted $\langle v_2\rangle_N$, gives rise to the flow modulation of the background shown in the figure.

To calculate the $\langle p_T\rangle$ of associated hadrons, the uncorrelated background is subtracted from both the p_T-weighted and number-weighted distributions before taking the ratio:

$$\langle p_T\rangle(\Delta\phi) = \frac{P_T(\Delta\phi) - B_{p_T}[1 + 2\langle v_2\rangle_{p_T}\cos(\Delta\phi)]}{N(\Delta\phi) - B_N[1 + 2\langle v_2\rangle_N\cos(\Delta\phi)]}, \quad (2)$$

where $N(\Delta\phi)$ and $P_T(\Delta\phi)$ are the same number-weighted and sum-p_T distributions used in Eq. (1), the average $\langle v_2\rangle$ are defined above, and B_{p_T} and B_N are background normalizations which are determined using the ZYAM method separately for the number and sum-p_T distributions.

Figure 8 shows the resulting $\langle p_T\rangle$ of associated hadrons as a function of $\Delta\phi$ in the away-side region for different centrality selections. In the peripheral bins, a peaked structure in $\langle p_T\rangle$ is found, similar to the results in d + Au collisions (open circles). With increasing centrality, the $\langle p_T\rangle$ around $\Delta\phi = \pi$ becomes lower. For the most central bin, the results show a minimum at $\Delta\phi = \pi$ for the two softer trigger selections. For the highest trigger selection $6 < p_T^{\rm trig} < 10\,{\rm GeV}/c$, a similar shape is seen, but there may be a slight enhancement at $\Delta\phi = \pi$ even in the most central collisions.

We further study the difference between $\langle p_T\rangle$ in the range $|\Delta\phi - \pi| < \frac{\pi}{6}$ (referred to as "core" in the following) and at $\frac{\pi}{6} < |\Delta\phi - \pi| < \frac{\pi}{2}$ (referred to as "cone" in the following). Figure 9 shows $\langle p_T\rangle$ in these two angular ranges as a function of the collision centrality for two different trigger p_T ranges. The $\langle p_T\rangle$ decreases with centrality approaching the inclusive $\langle p_T\rangle$, a feature already reported in Ref. [10] for associated hadrons in the entire away-side region ($|\Delta\phi - \pi| < 2.14$). This reduction of $\langle p_T\rangle$ is likely due to interactions with the medium. The fact that $\langle p_T\rangle$ approaches the $\langle p_T\rangle$ for inclusive particle production in events with a trigger hadron (solid lines in Fig. 9) may indicate that the associated particles at low p_T approach thermalization with the medium. It is also clear that the $\langle p_T\rangle$ of the core decreases more rapidly than that of the

cone hadrons, which suggests that there is significant transport of associated hadrons away from $\Delta\phi = \pi$ due to jet-medium interactions.

V. DISCUSSION AND CONCLUSIONS

In this paper, a comprehensive study of centrality and p_T dependence of azimuthal di-hadron correlations in Au + Au events is presented. We observe several striking modifications of the correlation structure in Au + Au compared to a d + Au reference. Associated yields on the near- and away-side are enhanced at lower p_T. On the near side, the increase in yield is partly located at large pseudorapidity difference $\Delta\eta$ (see Ref. [34] for a more detailed study) and the yields approach the measurement in d + Au collisions at the highest $p_T^{\rm trig}$. On the away side, the associated hadron distribution is significantly broadened; in fact, it is broad enough that it is impossible to unambiguously separate jetlike yields from the underlying event. At higher p_T, $p_T^{\rm assoc} > 2$ and $p_T^{\rm trig} > 6$ GeV/c, the away-side shape is narrow, like in d + Au events. A large enhancement of the away-side yield at low p_T is found, while at higher p_T a suppression is seen with respect to d + Au collisions.

These results are qualitatively consistent with a softening of jet fragmentation by in-medium energy loss, leading to an increase of the underlying parton energy selected by a trigger particle at given $p_T^{\rm trig}$. Some of the changes in the correlation shapes could then be due to fragmentation of radiated gluons.

The strong broadening of the away-side shapes, however, does not seem to fit naturally in a description of particle production from medium-modified jet fragmentation. Several alternative mechanisms have been proposed that could give rise to these structures. These can be divided into two categories: collective and radiative phenomena.

Radiative treatments [12,13,41,42,44] focus on the angular distribution of gluons radiated by the parton propagating through the medium. A large opening angle between the parent parton and radiated gluons is expected when kinematic constraints are imposed. Two simplified calculations of this effect have been published in the literature. One of these calculations gives results that are qualitatively consistent with the data [13], while the other calculation [12] shows a much smaller effect. Neither of the two calculations includes full integration over the initial-state kinematics and the medium density development. Another radiative scenario involves Cherenkov radiation of gluons [41,42,44], which would give rise to conical distributions.

Both for large-angle medium-induced gluon radiation and for gluon Cherenkov radiation, the expectation is that the away-side shape becomes narrower with increasing $p_T^{\rm assoc}$ [13,42]. This trend is not observed in the correlation data: using a few different functional forms for the away-side distributions, we found that peak-separation Δ is approximately independent of $p_T^{\rm assoc}$.

Alternatively, one could imagine that the passage of high-p_T partons excites sound waves in the medium. It has been suggested that this may lead to Mach shock waves [14–17]. Qualitatively, the observed constant separation between the away-side peak and the constant conical emission angle from three-particle correlations [40] are consistent with this explanation. The transition from a broad away-side structure at low p_T to a narrow structure at higher p_T would then signal the change from away-side structures dominated by bulk particle

TABLE I. v_2 and normalization values used for the background subtraction in Fig. 2.

$p_T^{\rm trig}$ (GeV/c)	$B_{\lvert\Delta\eta\rvert<2.0}$	$\langle v_2^{\rm assoc}\rangle\langle v_2^{\rm trig}\rangle$ (10^{-3})
	60–80%	
2.5–3.0	1.220 ± 0.002	20.6 ± 4.6
3.0–4.0	1.214 ± 0.003	19.4 ± 4.6
4.0–6.0	1.197 ± 0.008	15.7 ± 4.1
6.0–10.0	1.139 ± 0.026	8.67 ± 2.7
	40–60%	
2.5–3.0	3.846 ± 0.002	28.6 ± 4.4
3.0–4.0	3.835 ± 0.003	27.5 ± 4.6
4.0–6.0	3.820 ± 0.008	22.9 ± 4.5
6.0–10.0	3.76 ± 0.03	13.0 ± 3.2
	20–40%	
2.5–3.0	9.522 ± 0.002	25.9 ± 3.0
3.0–4.0	9.494 ± 0.003	25.4 ± 3.3
4.0–6.0	9.466 ± 0.008	21.8 ± 3.4
6.0–10.0	9.515 ± 0.031	12.8 ± 2.7
	0–12%	
2.5–3.0	23.531 ± 0.001	5.5 ± 1.5
3.0–4.0	23.469 ± 0.002	5.4 ± 1.6
4.0–6.0	23.395 ± 0.005	4.9 ± 1.5
6.0–10.0	23.365 ± 0.021	3.0 ± 1.1

TABLE II. v_2 values and normalization used for the background subtraction in Fig. 3.

$p_T^{\rm trig}$ (GeV/c)	$B_{\lvert\Delta\eta\rvert<2.0}$	$\langle v_2^{\rm assoc}\rangle\langle v_2^{\rm trig}\rangle$ (10^{-3})
	$0.5 < p_T^{\rm assoc} < 1.0$ GeV/c	
2.5–3.0	59.833 ± 0.002	2.9 ± 0.8
3.0–4.0	59.638 ± 0.003	2.8 ± 0.8
4.0–6.0	59.366 ± 0.009	2.6 ± 0.8
6.0–10.0	59.235 ± 0.034	1.6 ± 0.6
	$1.0 < p_T^{\rm assoc} < 1.5$ GeV/c	
2.5–3.0	17.286 ± 0.001	5.0 ± 1.4
3.0–4.0	17.238 ± 0.002	4.9 ± 1.4
4.0–6.0	17.182 ± 0.005	4.4 ± 1.4
6.0–10.0	17.154 ± 0.018	2.7 ± 1.0
	$1.5 < p_T^{\rm assoc} < 2.5$ GeV/c	
2.5–3.0	6.245 ± 0.001	6.8 ± 1.9
3.0–4.0	6.230 ± 0.001	6.6 ± 2.0
4.0–6.0	6.213 ± 0.003	6.0 ± 1.9
6.0–10.0	6.211 ± 0.011	3.7 ± 1.4
	$2.5 < p_T^{\rm assoc} < 4.0$ GeV/c	
2.5–3.0	0.5210 ± 0.0002	8.1 ± 2.4
3.0–4.0	0.5212 ± 0.0003	8.0 ± 2.5
4.0–6.0	0.5207 ± 0.0008	7.2 ± 2.4
6.0–10.0	0.5199 ± 0.0030	4.5 ± 1.7

production from the medium to a situation where jet fragments dominate.

A recent three-dimensional hydrodynamical calculation which includes local density fluctuations in the initial state also shows a broad away-side structure that may be consistent with the experimental di-hadron correlation data [29]. In this model, there is no explicit introduction of hard partons or jets; the correlation arises purely from the medium. At the moment, it is not clear whether this model will also generate the conical emission signal seen in three-particle correlation data [40]. A study of three-particle correlations in this model is ongoing [45].

In general, a number of different mechanisms, including fragmentation, radiative energy loss, bulk response, and hadron formation by coalescence of constituent quarks, may contribute to the observed di-hadron correlation structures. Quantitative modeling of the different processes, including the azimuthal correlation of the trigger and associated hadrons with the reaction plane, is needed to further disentangle the observed signals and the background.

Experimentally, more insight in the underlying production processes will be gained from di-hadron measurements with identified particles and with respect to the reaction plane. In addition, γ-jet measurements, and measurements with reconstructed jets are being pursued, which provide better control over the initial-state kinematics.

ACKNOWLEDGMENTS

We thank the RHIC Operations Group and RCF at BNL, the NERSC Center at LBNL, and the Open Science Grid consortium for providing resources and support. This work was supported in part by the Offices of NP and HEP within the US DOE Office of Science, the US NSF, the Sloan Foundation, the DFG cluster of excellence 'Origin and Structure of the Universe' of Germany, CNRS/IN2P3, STFC, and EPSRC of the United Kingdom, FAPESP CNPq of Brazil, Ministry of Ed. and Sci. of the Russian Federation, NNSFC, CAS, MoST, and MoE of China, GA and MSMT of the Czech Republic, FOM and NWO of the Netherlands, DAE, DST, and CSIR of India, Polish Ministry of Sci. and Higher Ed., Korea Research Foundation, Ministry of Sci., Ed. and Sports of the Rep. of Croatia, Russian Ministry of Sci. and Tech, and RosAtom of Russia.

APPENDIX: BACKGROUND SHAPES

In this Appendix, we show the associated hadron azimuthal distributions before subtracting the flow background.

Figure 10 shows the distributions for associated particles between 1.0 and 2.5 GeV/c and for different ranges of trigger particle p_T, ranging from 2.5–3.0 GeV/c (left column) to 6–10 GeV/c (right column) and different centralities (rows). Note the large increase of the combinatorial background with centrality. A large background modulation due to elliptic flow is expected.

Figure 11 shows the distributions of associated charged particles with various $p_T^{\rm assoc}$ and $p_T^{\rm trig}$ selections for 0–12% central Au + Au collisions. For $p_T^{\rm assoc} > 1.0$ GeV/c (lower three rows), the value of $(1/N_{\rm trig})\, dN/d\Delta\phi$ at the minimum depends mostly on $p_T^{\rm assoc}$, as expected for uncorrelated background. In the upper row, however, with $0.5 < p_T^{\rm assoc} < 1.0$ GeV/c, we observe a significant dependence of $(1/N_{\rm trig})\, dN/d\Delta\phi$ at the minimum on $p_T^{\rm trig}$. The value at the minimum increases for lower $p_T^{\rm trig}$, which is qualitatively consistent with a centrality bias combined with the fact that the probability to find more than one trigger particle per event is sizable for the lower $p_T^{\rm trig}$ selections and decreases with increasing $p_T^{\rm trig}$.

The background normalization (B) and the elliptic flow $\langle v_2^{\rm assoc}\rangle\langle v_2^{\rm trig}\rangle$ that were used to subtract the background in Figs. 2 and 3 are reported in Tables I and II.

[1] J. Adams *et al.* (STAR Collaboration), Phys. Rev. Lett. **91**, 072304 (2003).
[2] M. Gyulassy and M. Plumer, Phys. Lett. B **243**, 432 (1990).
[3] X.-N. Wang and M. Gyulassy, Phys. Rev. Lett. **68**, 1480 (1992).
[4] R. Baier, Y. L. Dokshitzer, A. H. Mueller, S. Peigne, and D. Schiff, Nucl. Phys. B **483**, 291 (1997).
[5] C. Adler *et al.* (STAR Collaboration), Phys. Rev. Lett. **89**, 202301 (2002).
[6] K. Adcox *et al.* (PHENIX Collaboration), Phys. Rev. Lett. **88**, 022301 (2001).
[7] J. Adams *et al.* (STAR Collaboration), Phys. Rev. Lett. **97**, 162301 (2006).
[8] C. Loizides, Eur. Phys. J. C **49**, 339 (2007).
[9] H. Zhang, J. F. Owens, E. Wang, and X.-N. Wang, Phys. Rev. Lett. **98**, 212301 (2007).
[10] J. Adams *et al.* (STAR Collaboration), Phys. Rev. Lett. **95**, 152301 (2005).
[11] A. Adare *et al.* (PHENIX Collaboration), Phys. Rev. C **78**, 014901 (2008).
[12] I. Vitev, Phys. Lett. B **630**, 78 (2005).
[13] A. D. Polosa and C. A. Salgado, Phys. Rev. C **75**, 041901 (2007).
[14] H. Stoecker, Nucl. Phys. A **750**, 121 (2005).
[15] J. Casalderrey-Solana, E. V. Shuryak, and D. Teaney, J. Phys. Conf. Ser. **27**, 22 (2005).
[16] T. Renk and J. Ruppert, Phys. Rev. C **73**, 011901 (2006).
[17] J. Ruppert and B. Muller, Phys. Lett. B **618**, 123 (2005).
[18] R. C. Hwa and C. B. Yang, Phys. Rev. C **66**, 025205 (2002).
[19] R. J. Fries, B. Muller, C. Nonaka, and S. A. Bass, Phys. Rev. Lett. **90**, 202303 (2003).
[20] V. Greco, C. M. Ko, and P. Levai, Phys. Rev. Lett. **90**, 202302 (2003).
[21] K. H. Ackermann *et al.* (STAR Collaboration), Nucl. Instrum. Methods A **499**, 624 (2003).
[22] M. Anderson *et al.*, Nucl. Instrum. Methods A **499**, 659 (2003).
[23] F. S. Bieser *et al.* (STAR Collaboration), Nucl. Instrum. Methods A **499**, 766 (2003).
[24] J. Adams *et al.* (STAR Collaboration), Phys. Rev. C **72**, 014904 (2005).
[25] N. N. Ajitanand *et al.*, Phys. Rev. C **72**, 011902 (2005).

[26] J. Adams *et al.* (STAR Collaboration), Phys. Rev. C **75**, 034901 (2007).
[27] T. A. Trainor, Phys. Rev. C **81**, 014905 (2010).
[28] S. A. Voloshin, Phys. Lett. B **632**, 490 (2006).
[29] J. Takahashi *et al.*, Phys. Rev. Lett. **103**, 242301 (2009).
[30] J. Liao and E. Shuryak, Phys. Rev. C **77**, 064905 (2008).
[31] A. Dumitru, F. Gelis, L. McLerran, and R. Venugopalan, Nucl. Phys. A **810**, 91 (2008).
[32] S. Gavin, L. McLerran, and G. Moschelli, Phys. Rev. C **79**, 051902 (2009).
[33] J. Adams *et al.* (STAR Collaboration), Phys. Rev. C **73**, 064907 (2006).
[34] B. I. Abelev *et al.* (STAR Collaboration), Phys. Rev. C **80**, 064912 (2009).
[35] B. I. Abelev *et al.* (STAR Collaboration), Phys. Rev. Lett. **105**, 022301 (2010).
[36] R. C. Hwa and C. B. Yang, Phys. Rev. C **70**, 024905 (2004).
[37] C. B. Chiu and R. C. Hwa, Phys. Rev. C **72**, 034903 (2005).
[38] A. Adare *et al.* (PHENIX Collaboration), Phys. Lett. B **649**, 359 (2007).
[39] S. S. Adler *et al.* (PHENIX Collaboration), Phys. Rev. C **71**, 051902 (2005).
[40] B. I. Abelev *et al.* (STAR Collaboration), Phys. Rev. Lett. **102**, 052302 (2009).
[41] A. Majumder and X.-N. Wang, Phys. Rev. C **73**, 051901 (2006).
[42] V. Koch, A. Majumder, and X.-N. Wang, Phys. Rev. Lett. **96**, 172302 (2006).
[43] S. Zhang *et al.*, Phys. Rev. C **76**, 014904 (2007).
[44] I. M. Dremin, JETP Lett. **30**, 140 (1979).
[45] R. P. G. Andrade, F. Grassi, Y. Hama, and W. L. Qian, J. Phys. G **37**, 094043 (2010).